Residual Monte Carlo with Discrete Scattering Angles in the 1-D Transport Equation

Brian C. Franke[1], Don E. Bruss[1,2], and Jim E. Morel[2]

[1]*Sandia National Laboratories, Albuquerque, NM 87185, USA*
[2]*Department of Nuclear Engineering, Texas A&M University, College Station, TX 77843, USA*
bcfrank@sandia.gov, brussd@tamu.edu; morel@tamu.edu

INTRODUCTION

The accuracy of the Monte Carlo method is often undermined by its precision limitations. The statistical error converges only at a rate inversely proportional to the square root of the number of particle histories. It has long been known that exponential convergence can be achieved using an iterative residual Monte Carlo technique [1, 2, 3]. Practical implementations of this method have had the same discretization errors as deterministic methods [4, 5]. Residual Monte Carlo implementations for the continuous transport equation have been limited to the two-stream transport equation [6], four-stream transport equation [7], and isotropic scattering [8, 9]. Building on the approach developed by Morel et al. [6, 9] of using piecewise-linear finite-element trial spaces, we demonstrate exponential convergence for anisotropic scattering kernels composed of discrete scattering angles.

We first develop an expression for a scattering matrix that is used in the evaluation of the scattering source in the calculation the residual. We employ numerical integration to precompute the required scattering matrix for a discrete scattering angle. The results demonstrate that the method is capable of converging to machine precision when the solution lies within the trial space. When the solution does not lie within the trial space, we demonstrate that mesh refinement permits greater accuracy to be achieved before exponential convergence stagnates. Finally, we characterize the behavior of the algorithm for various convergence criteria used in the numerical integration of the scattering matrices.

RESIDUAL MONTE CARLO METHOD

The continuous 1-D transport equation with anisotropic scattering is:

$$\mu\frac{\partial\psi(\mu,z)}{\partial z}+\sigma_t\psi(\mu,z)=q \\ +\frac{1}{4\pi}\int_0^{2\pi}\int_{-1}^{1}\sigma_s(\mu_0)\psi(\mu',z)d\mu' d\phi', \qquad (1)$$

for $\mu\in[-1,1]$ and $z\in[0,T]$. μ is the direction cosine with respective to the z-axis, $\psi(\mu,z)$ is the angular flux, σ_t is the total interaction cross section, σ_s is the scattering cross section, $\mu_0=\vec{\Omega}'\cdot\vec{\Omega}$ is the cosine of the scattering angle, and q is a distributed source.

We can express the transport equation as:

$$\mathbf{L}\psi=q, \qquad (2)$$

where $\mathbf{L}$ is the transport operator. The residual Monte Carlo algorithm is then expressed in terms of an iteration index, n:

$$r^{(n)}=q-\mathbf{L}\psi^{(n-1)}, \qquad (3)$$

$$\mathbf{L}\epsilon^{(n)}=r^{(n)}, \qquad (4)$$

$$\psi^{(n)}=\psi^{(n-1)}+\epsilon^{(n)}. \qquad (5)$$

Eq. (4) is solved using a standard Monte Carlo radiation transport code with a distributed source specified by the residual r and tallying a flux correction, ϵ, on linear finite-element basis functions. Eq. (5) is a trivial addition of the flux correction to the previous estimate of the flux. The difficulty of the residual Monte Carlo method is that the residual calculation in Eq. (3) must be evaluated precisely and must be consistent with the transport operator as applied by the Monte Carlo code in Eq. (4). The contribution of each term from Eq. (1) must be included in the residual evaluation. Using the integro-differential form of the transport equation rather than the integral form often associated with Monte Carlo calculations, this is a local operation, which is simplified by predetermining that the flux will be represented only on linear discontinuous basis functions.

Within each finite-element cell, the flux is represented on a linear basis:

$$\psi_{i,m}=\psi^a_{i,m}+\psi^z_{i,m}\frac{2}{h_i}(z-z_i)+\psi^\mu_{i,m}\frac{2}{h_m}(\mu-\mu_m). \qquad (6)$$

ψ^a, ψ^z, and ψ^μ denote the average, z-slope, and μ-slope of the angular flux, respectively. z_i and μ_m are the respective cell midpoints. h_i and h_m are the respective cell widths. The extent of each cell is $\mu\in[\mu_{m-1/2},\mu_{m+1/2}]$, with $z\in[z_{i-1/2},z_{i+1/2})$ for $\mu<0$ and $z\in(z_{i-1/2},z_{i+1/2}]$ for $\mu>0$. Here we will consider only uniform cells with M angular regions and I spatial regions, with $\mu_{1/2}=-1$, $\mu_{M+1/2}=1$, $z_{1/2}=0$, and $z_{I+1/2}=T$.

The residual for each cell is given by

$$r_{i,m}=-\mu\frac{\partial\psi_{i,m}}{\partial z}-\sigma_{t,i}\psi_{i,m}+q_{i,m}+\sigma_{s0,i}s_{i,m}, \qquad (7)$$

$$s_{i,m}=\int_0^{2\pi}\int_{-1}^{1}p(\mu_0)\psi_i(\mu')d\mu' d\phi', \qquad (8)$$

where $\sigma_{s0,i}$ is the total scattering cross section, which combined with $s_{i,m}$ is the scattering source. (The projection of the scattering integral onto the trial space for $s_{i,m}$ is implicit here but will be included explicitly later.) $p(\mu_0)$ is the pdf of the scattering distribution, and

$$\psi_i(\mu) = \sum_{m=1}^{M} \psi_{i,m} \Pi_{m-\frac{1}{2},m+\frac{1}{2}}(\mu), \tag{9}$$

where $\Pi_{a,b}$ is the boxcar function.

The residual terms containing the total cross section and source are trivial operations. The spatial gradiant has previously been discussed in detail [9] as resulting in two components: one within the cell and one at the cell's spatial boundaries. Differentiating Eq. (6) with respect to z, there is a linear term within the cell given by

$$\mu \frac{\partial \psi_{i,m}}{\partial z} = \mu_m \frac{2}{h_i} \psi^z_{i,m} + (\mu - \mu_m) \frac{2}{h_i} \psi^z_{i,m}, \tag{10}$$

for $z \in (z_{i-1/2}, z_{i+1/2})$. At the cell boundary, there is a delta function in space based on any discontinuity of fluxes between the cell and an upwind cell (or boundary condition). For example, for the $\mu > 0$ direction with an adjacent upwind cell, this is

$$\mu \frac{\partial \psi_{i,m}}{\partial z} = \mu \left[\psi_{i,m}(z_{i-\frac{1}{2}}, \mu) - \psi_{i-1,m}(z_{i-\frac{1}{2}}, \mu) \right], \tag{11}$$

at $z = z_{i-1/2}$. This term results in a quadratic in μ. Operationally, only the linear flux and source variations are included in the residual at cell spatial boundaries and the μ weighting is included explicitly when calculating the residual source strength and when sampling particles at cell edges.

In residual calculations, the source due to scattering has previously been modeled with isotropic scattering, which is also relatively straightforward to evaluate. To include anisotropic scattering, we must evaluate the scattering integral. We discuss this scattering source in the following section.

SCATTERING SOURCE EVALUATION

Omitting the leading total scattering cross section in the following discussion, the scattering source in cell i before projection onto the linear discontinuous basis is

$$S_i(\mu) = \int_0^{2\pi} \int_{-1}^{1} p(\mu_0) \psi_i(\mu') d\mu' d\phi'. \tag{12}$$

Discrete scattering angles are often used in multigroup Monte Carlo codes [10], so we begin by considering only a single discrete scattering angle, μ_* in the polar deflection angle, μ_0 (with scattering still uniform in the azimuthal deflection angle).

$$S_i(\mu) = \int_0^{2\pi} \int_{-1}^{1} \frac{\delta(\mu_0 - \mu_*)}{2\pi} \psi_i(\mu') d\mu' d\phi'. \tag{13}$$

To perform the integration it is easiest to map into the scattering frame.

$$S_i(\mu) = \int_0^{2\pi} \int_{-1}^{1} \frac{\delta(\mu_0 - \mu_*)}{2\pi} \psi_i(\phi_0) d\mu_0 d\phi_0. \tag{14}$$

One can show the following relationship between the lab-frame and scattering-frame angles:

$$\mu' = \mu\mu_0 + \sqrt{1-\mu^2}\sqrt{1-\mu_0^2}\cos(\phi_0 - \phi'). \tag{15}$$

Since ψ is not a function of ϕ', we can simplify to consider only $\cos(\phi_0) = \cos(\phi_0 - \phi')$. Thus, Eq. (14) becomes

$$S_i(\mu) = \frac{1}{\pi} \int_0^{\pi} \psi_i(\mu\mu_* + \sqrt{1-\mu^2}\sqrt{1-\mu_*^2}\cos(\phi_0)) d\phi_0. \tag{16}$$

The integral must be evaluated using the discontinuous representation of ψ, with the discontinuities mapped using the relationship given in Eq. (15) to determine each integration range $[\phi_{j-1/2}, \phi_{j+1/2}]$ corresponding to $[\mu_{m'-1/2}, \mu_{m'+1/2}]$ cell boundaries but with some cells omitted or truncated due to the $[0, \pi]$ integration range in ϕ_0. (We introduce the m' subscript to distinguish the indexing of μ' from the m indexing of the μ variable.) $S_i(\mu)$ must also be projected onto the linear basis. In our implementation, we evaluate these integrations separately for unit coefficients of the average, z-slope, and μ-slope terms for each integration range of ψ projected onto the integration range for each coefficient of the scattering source, $s_{i,m}$. These integrations take the following form:

$$\begin{aligned} S^{x,y}_{i,m,m'} \quad = \quad & \frac{1}{\pi} \int_{z_{i-\frac{1}{2}}}^{z_{i+\frac{1}{2}}} \frac{1}{h_i} \left(\frac{z - z_i}{h_i/6} \right)^k \times \\ & \int_{\mu_{m-\frac{1}{2}}}^{\mu_{m+\frac{1}{2}}} \frac{1}{h_m} \left(\frac{\mu - \mu_m}{h_m/6} \right)^\ell \times \\ & \int_{\phi_{j-\frac{1}{2}}}^{\phi_{j+\frac{1}{2}}} \psi^x_i(\phi_0, z, \mu) d\phi_0 d\mu dz, \end{aligned} \tag{17}$$

where x and y indicate the average or slope superscripts a, z, or μ for the flux and the projection of the scattering source, respectively. The projections are: for $y = a$, $k = 0$ and $\ell = 0$; for $y = z$, $k = 1$ and $\ell = 0$; and for $y = \mu$, $k = 0$ and $\ell = 1$. Eq. (17) provides the elements of a scattering matrix that can be used to project the flux coefficients, $\psi_{i,m'}$, onto the scattering source coefficients for calculating the residual: $s^y_{i,m} = S^{x,y}_{i,m,m'} \psi^x_{i,m'}$. In our implementation, we evaluate the integrals using Gauss-Legendre quadrature with increasing order until a convergence tolerance, τ, is met for all elements of the matrix. The scattering matrix can be precomputed, since it is independent of the fluxes and depends only on the scattering distribution and angular divisions of the trial space.

NUMERICAL RESULTS

Our first test problem has a uniform flux solution. This problem is convenient, because even with a discrete scattering angle the solution lies in the trial space. We calculate the source from the specified flux solution by the method of manufactured solutions,

$$q = \mathbf{L}\psi, \tag{18}$$

using the same code that is needed to calculate the residual. For this test problem, $\sigma_t = 1$, $\sigma_s 0 = 0.9$, $\mu_* = 0.8$, $T = 3$, and $\tau = 0.01$. We use 100 cells in a 10×10 uniform grid. Calculations were performed with varying numbers of histories per cycle ("H/C"), where a "cycle" is one iteration in the residual calculation. In Fig. 1 we show the relative L2-norm of error as a function of the number of cycles. The results with 1000 histories per cycle diverge because the statistical error is too large to permit a sufficiently accurate residual calculation. The results also show that increasing the number of histories per cycle increases the rate of convergence per cycle.

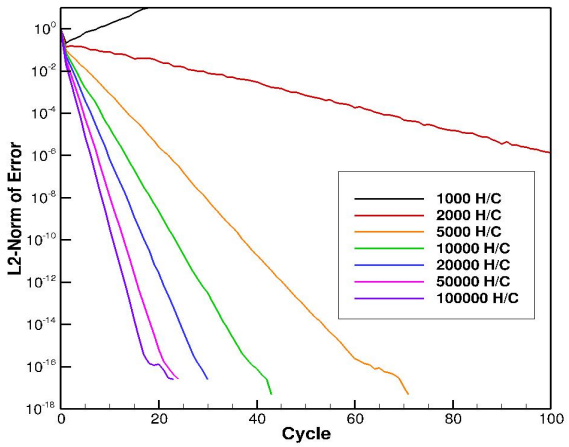

Fig. 1: Exponential convergence of error versus number of cycles for a uniform solution problem with varying numbers of histories per cycle.

In Fig. 2, we show the relative L2-norm of error as a function of the number of histories. This figure has some of the same results as Fig. 1 plotted on a log-log scale and includes the error for standard Monte Carlo with $1/\sqrt{N}$ convergence for comparison. These results show that, using number of histories as a reasonable approximation for runtime, there is an optimal number of histories per cycle to achieve the fastest convergence.

Our second test problem uses an angular scattering distribution based on the cross section for 1 MeV electrons in water. We use $\sigma_t = 77$, $\sigma_s 0 = 76.9$, $T = 10$, $\tau = 0.01$, and four discrete scattering angles with direction cosines of 0.98, 0.56, -0.19, and -0.82 and probabilities of 0.9916, 0.0070, 0.0011, and 0.0003, respectively.

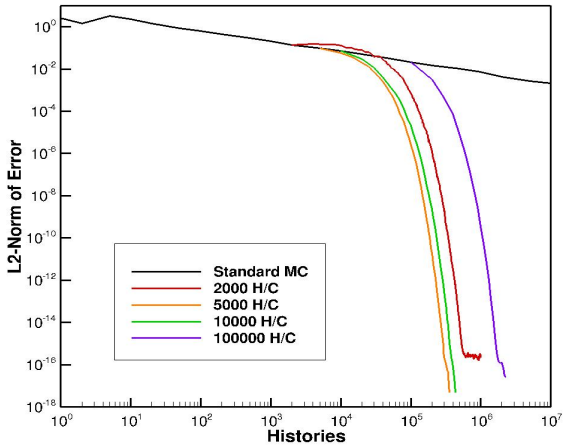

Fig. 2: Exponential convergence of error versus number of histories for a uniform solution problem with varying numbers of histories per cycle compared to standard Monte Carlo convergence.

A unit isotropic flux is incident on the slab at $z = 0$. We varied the number of cells in the problem, while keeping a fixed 100 histories per cycle per cell and using an $N \times N$ grid with the same number of cell divisions in space and angle. The converged results are shown in Fig. 3 for the 128×128 grid.

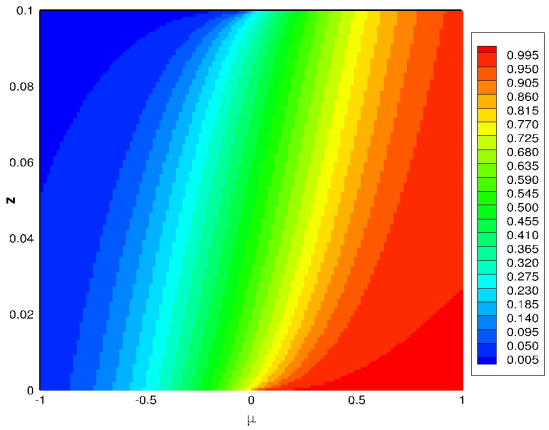

Fig. 3: Angular flux distribution for the second test problem.

For this problem, we report the L2-norm of the residual, since the exact solution is not known. Fig. 4 shows the expected behavior, exponential convergence to a saturation point at which the trial space is inadequate to permit a more accurate solution. As the trial space is refined, the saturation of convergence occurs at a lower level of error.

Our studies varying tolerance τ on these problems showed that even low-order quadrature produced accurate results with no discernable effect on convergence rate. Studies on more difficult problems are warranted.

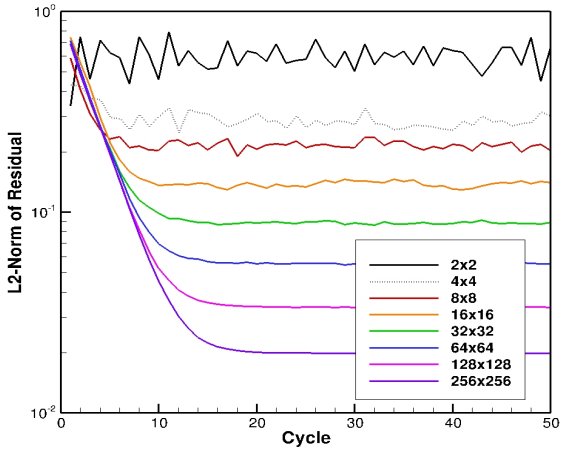

Fig. 4: Exponential convergence of residual versus number of cycles for an anisotropic scattering problem with varying uniform refinement of the trial space.

CONCLUSIONS

The residual Monte Carlo method is a powerful technique for expected value problems involving Markov processes. These results demonstrate that it can be successfully applied to the continuous 1-D transport equation with anisotropic scattering. Since the method can be initialized with an approximate solution and is compatible with particle biasing techniques commonly used in Monte Carlo calculations, it seems well suited to further accelerate techniques like FW-CADIS [11], in which a coarse deterministic forward solution and adjoint-based biasing can be leveraged.

However, research issues remain. One could further integrate the scattering angle over a continuous scattering distribution to apply the approach to general anisotropic scattering. The scattering source evaluation and the residuals due to flux discontinuities at cell boundaries need to be extended to 2-D and 3-D. Though we have not yet demonstrated a multigroup implementation, that appears to be a minor extension from the monoenergetic implementation here. Extension to continuous energy will be a more difficult effort but may use a similar approach to the one developed here. For a production capability it will desirable to include adaptive refinement of the trial space [9], which may require better understanding of how to manage particle populations in highly refined regions.

ACKNOWLEDGEMENTS

Supported by the Laboratory Directed Research and Development program at Sandia National Laboratories, a multi-program laboratory managed and operated by Sandia Corporation, a Lockheed Martin Company, for the United States Department of Energy, under contract DE-AC04-94AL85000.

REFERENCES

[1] J. H. HALTON, "Sequential Monte Carlo," *Proc. Camb. Phil. Soc.*, **58**, 57-78 (1962).

[2] J. A. FAVORITE, H. LICHTENSTEIN, "Exponential Monte Carlo Convergence of a Three-Dimensional Discrete Ordinates Solution," *Trans. Am. Nucl. Soc.*, **81**, 147-148 (1999).

[3] H. LICHTENSTEIN, "Exponential Convergence Rates For Reduced-Source Monte Carlo Transport in [X,Y] Geometry," **133**, 258-268 (1999).

[4] T. M. EVANS, et al., "A Residual Monte Carlo Method For Discrete Thermal Radiation Diffusion," *J. Comp. Phys.*, **189**, 539-556 (2003).

[5] T. M. EVANS, S. W. MOSHER, "A Monte Carlo Synthetic Acceleration Method for the Non-Linear, Time-Dependent Diffusion Equation," *Int. Conf. on Math., Comp. Methods & Reactor Phys. (M&C 2009)*, Saratoga Springs, New York, May 3-7 (2009).

[6] J. E. MOREL, J. P. TOOLEY, B. J. BLAMER, "Exponentially-Convergent Monte Carlo Via Finite-Element Trial Spaces," *Int. Conf. on Math. and Comp. Methods Applied to Nucl. Sci. and Eng. (M&C 2011)*, Rio de Janeiro, RJ Brazil, May 8-12 (2011).

[7] R. KONG, J. SPANIER, "Geometric Convergence of Second Generation Adaptive Monte Carlo Algorithms for General Transport Problems Based on Correlated Sampling," *Int. J. Pure App. Maths.*, **59**, 4, 435-455 (2010).

[8] R. T. WOLLAEGER, J. D. DENSMORE, "A Residual Monte Carlo Method for Spatially Discrete, Angularly Continuous Radiation Transport," *Trans. Am. Nucl. Soc.*, **106**, 335-338 (2012).

[9] J. R. PETERSON, J. E. MOREL, J. C. RAGUSA, "Exponentially-Convergent Monte Carlo for the 1-D Transport Equation," *Int. Conf. on Math. and Comp. Methods Applied to Nucl. Sci. and Eng. (M&C 2013)*, Sun Valley, Idaho, May 5-9 (2013).

[10] J.E. MOREL, et al., "A Hybrid Multigroup/Continuous-Energy Monte Carlo Method for Solving the Boltzmann-Fokker-Planck Equation," *Nucl. Sci. and Eng.*, **124**, 369-389 (1996).

[11] D. E. PEPLOW, "Comparison of Hybrid Methods for Global Variance Reduction in Shielding Calculations," *Trans. Am. Nucl. Soc.*, **107**, 512-515 (2012).